Capilla Romá, MT.; Talavera Usano, CF.; Ginestar Peiro, D.; Verdú Martín, GJ. (2012). Application of a nodal collocation approximation for the multidimensional P-L equations to the 3D Takeda benchmark problems. Annals of Nuclear Energy. 40(1):1-13. doi:10.1016/j.anucene.2011.09.014.

Application of a nodal collocation approximation for the multidimensional P_L equations to the 3D Takeda benchmark problems

M. Capilla [a] C. F. Talavera [a] D. Ginestar [a] G. Verdú [b,*]

[a] *Departamento de Matemática Aplicada. Universidad Politécnica de Valencia. Camino de Vera 14. E-46022 Valencia, Spain.*

[b] *Departamento de Ingeniería Química y Nuclear. Universidad Politécnica de Valencia. Camino de Vera 14, E-46022 Valencia, Spain.*

Abstract

P_L equations are classical approximations to the neutron transport equations, which are obtained expanding the angular neutron flux in terms of spherical harmonics. These approximations are useful to study the behavior of reactor cores with complex fuel assemblies, for the homogenization of nuclear cross sections, etc., and most of these applications are in three-dimensional (3D) geometries. In this work, we review the multi-dimensional P_L equations and describe a nodal collocation method for the spatial discretization of these equations for arbitrary odd order L, which is based on the expansion of the spatial dependence of the fields in terms of orthonormal Legendre polynomials. The performance of the nodal collocation method is studied by means of obtaining the k_{eff} and the stationary power distribution of several 3D benchmark problems. The solutions are obtained are compared with a finite element method and a Monte Carlo method.

Key words: Multidimensional P_L equations; Nodal collocation method; Lambda Modes transport problem; Three-dimensional neutron transport benchmark.

* Corresponding author. Tel.: 34-963877630; fax: 34-963877639.
Email addresses: tcapilla@mat.upv.es (M. Capilla), talavera@mat.upv.es (C. F. Talavera), dginesta@mat.upv.es (D. Ginestar), gverdu@iqn.upv.es (G. Verdú).

1 Introduction

For reactor calculations the neutron multi-group transport problem is usually treated using the classical diffusion approximation, but this approximation does not provide good results for complex fuel assemblies or other applications as fine mesh (pin by pin) geometry. To improve the angular dependency, deterministic methods such as discrete ordinates (S_N), spherical harmonics (P_L) and method of characteristics or, alternatively, Monte Carlo methods can be used.

The discrete ordinates method (S_N) is implemented in several codes such as DANTSYS (Alcouffe et al., 1995), PENTRAN (Sjoden and Haghighat, 1996) and DORT/TORT (Rhoades and Childs, 1993). The main drawback of S_N codes are ray-effects (unphysical numerical analysis obtained in scalar fluxes, which may have important effects in the solution). The Monte Carlo methods do not provide complete flux solutions to the whole problem geometry requiring additional computational burden (Briesmeister, 2000). Nevertheless, these methods work very well to obtain integral quantities (k_{eff}, dose rate, etc.). The method of characteristics (DeHart, 2009) are becoming very popular, but their main drawback is the computational cost. The P_L approximation to the transport equation is well established (Davison, 1957; Weinberger and Wigner, 1958; Clark and Hansen, 1964) and is obtained by expanding the angular dependence of the nuclear flux and the neutron cross-sections in terms of spherical harmonics up to a finite-order L. The exact transport equation is recovered as L goes to infinity. In three-dimensional geometries (3D), the equations are complicated and can be formulated as second-order differential equations, but the coupling involves not only the angular moments but also mixed spatial derivatives of these moments. These problems led to propose the simplified P_L (SP_L) approximation (Gelbard, 1968), where the second derivatives in the one-dimensional planar geometry P_L equations are replaced by three-dimensional Laplacian operators, avoiding the complexity of the full spherical approximation.

In the 90s theoretical basis for the observed accuracy of the SP_L equations in the multi-dimensional applications were provided (Brantley and Larsen, 2000) showing that these equations are high-order asymptotic solutions of the transport equations. The SP_L equations are a practical way to solve transport problems in simplified physical systems, but when applied to general 3D transport problems the accuracy of the solution can not be increased with larger L order, and it is possible to obtain worse results with the SP_L approximation than with the diffusion equation (Tomasević and Larsen, 1996). The best solution is obtained from the P_L approximation, but its implementation in a computer program is complicated. Fletcher (1983) obtained a solution of the P_L equations eliminating the fields with odd-order and discretizing the result-

ing equations using the finite difference or finite element method. Recently, in the work of Ziver et al. (2005) the spherical harmonics (P_L) equations are solved using finite elements methods and implemented in the code EVENT. To qualify the numerical methods and algorithms, three benchmark problems (Takeda and Ikeda, 1991) were computed and results were compared against the Monte Carlo code MCNP4C (Briesmeister, 2000).

In a previous work (Capilla et al., 2008) the authors developed a nodal collocation approximation for P_L equations that made use of some practical simplifications appropriate for most 2D applications. The performance of the method was checked for some 2D test cases and computation results agreed well with reference results. However, for precise computations in 2D geometries and for 3D applications the full theory is required to obtain accurate results, at the price of a more complicated set of equations.

In this work, we review the multi-dimensional P_L equations and describe a nodal collocation method for the spatial discretization of these equations for arbitrary odd order L, which is based on the expansion of spatial dependence of the fields in terms of orthonormal Legendre polynomials. The nodal collocation method approximates the initial differential eigenvalue problem by a generalized algebraic eigenvalue problem from which the k-effective and the stationary neutron flux distribution of the system can be computed, being able also to obtain the subcritical eigenvalues and their corresponding eigenmodes. The P_L nodal collocation method has been implemented into a computer code called SHNC (Spherical Harmonics Nodal Collocation). The main advantage of the method developed in this paper is the lower dimension and good characteristics of the matrix associated to the algebraic problem. The dimension increases with the order L of the spherical harmonics expansion as $L(L+1)/2$ and with the order of the Legendre polynomials used in the nodal collocation method, but the serendipity approximation and the possibility of using nodes of big size (i.e. 15 cm x 15 cm) reduces drastically the dimension of the algebraic problem in comparison with other methods as finite elements or finite differences.

Two kind of boundary conditions are considered. Vacuum boundary conditions are approximated to finite order L by setting Marshak's conditions. The resulting set of conditions is overdetermined but a canonical procedure is applied to reduce the number of conditions. Reflecting boundary conditions are also described and they are computed in an exact way.

The SHNC code has been tested first by solving 2D and 3D homogeneous eigenvalue problems with small length side. The results are then compared with the ones obtained from DANTSYS code (TWODANT and THREEDANT, Alcouffe et al. (1995)). More realistic cases are then studied and two 3D benchmark eigenvalue problems (Takeda and Ikeda, 1991) are solved.

Results are compared with the ones obtained with the finite element code EVENT (Ziver et al., 2005), the Monte Carlo code MCNP4C and also with the results summarized in the NCRP Technical Report (Takeda and Ikeda, 1991).

The rest of the paper is organized as follows. In Section 2, we review the spherical harmonics method that, when applied to the transport equation eigenvalue problem, gives the multi-dimensional P_L equations. These equations can be formulated as vector-valued second order differential equations. The spherical harmonics method is also applied to vaccum and reflective boundary conditions. In Section 3, the spatial discretization of P_L equations is done using a nodal collocation method that is based on the expansion of the fields in terms of Legendre polynomials. This procedure will approximate the transport equation eigenvalue problem by an algebraic generalized eigenvalue problem. In Section 4 the performance of the method is validated with 2D and 3D homogeneous one-group isotropic eigenvalue problems and also with realistic 3D multi-group neutron transport benchmark problems proposed by Takeda et al. (1988). Finally, in Section 5 we establish our conclusions.

2 The transport equation and the P_L equations

In this section we review the multi-dimensional P_L equations, for arbitrary angular order L, that will be formulated as vector-valued second order differential equations. Boundary conditions will also be computed for arbitrary order L. Vacuum boundary conditions are approximated using Marshak's conditions. On the contrary, reflecting boundary conditions can be treated in an exact way.

We will concentrate on the transport equation eigenvalue problem (Stacey, 2001)

$$\begin{aligned}\vec{\Omega}\ \vec{\nabla}\Phi(\vec{r},\vec{\Omega},E) + \Sigma_t(\vec{r},E)\,\Phi(\vec{r},\vec{\Omega},E) \\ = \int dE' \int d\vec{\Omega}'\,\Sigma_s(\vec{r};\vec{\Omega}',E'\to\vec{\Omega},E)\,\Phi(\vec{r},\vec{\Omega}',E') \\ + \frac{1}{\lambda}\frac{\chi_p(E)}{4\pi}\int dE'\,\nu\Sigma_f(\vec{r},E')\int d\vec{\Omega}'\,\Phi(\vec{r},\vec{\Omega}',E')\ ,\end{aligned} \tag{1}$$

known as the *Lambda Modes transport problem*. Here $\Phi(\vec{r},\vec{\Omega},E)$ is the angular neutronic flux at location $\vec{r}$ with energy E and direction given by the unit vector $\vec{\Omega}$; Σ_t is the total cross-section; Σ_s is the scattering cross section from $(\vec{\Omega}',E')$ to $(\vec{\Omega},E)$; Σ_f is the fission cross-section; ν is the average number of neutrons per fission and χ_p is the spectrum. Nevertheless, the same kind of

method is also valid for other kind of problems such as stationary problems with neutron sources.

In practical applications, to eliminate the dependence of energy in Eq. (1), an energy multi-group approximation is used. In order to facilitate the notation we will consider the monoenergetic version of these equations. For the extension of the nodal collocation method to the case of G energy groups, $\Phi(\vec{r},\vec{\Omega})$ is replaced by a column vector of G components corresponding to each energy group, Σ_t is a diagonal matrix and Σ_s, $\nu\Sigma_f$ are also adequate matrices.

In the spherical harmonics method the angular dependence of the angular neutronic flux $\Phi(\vec{r},\vec{\Omega})$ is expanded in terms of spherical harmonics $Y_l^m(\vec{\Omega})$,

$$\Phi(\vec{r},\vec{\Omega}) = \sum_{l=0}^{\infty} \sum_{m=-l}^{+l} \phi_l^m(\vec{r})\, Y_l^m(\vec{\Omega}) \ , \tag{2}$$

where $\phi_l^m(\vec{r})$ are the (spherical harmonics) moments. It will also be assumed that scattering depends only on the relative angle between the incident and the scattered neutrons, $\mu_0 = \vec{\Omega}\,\vec{\Omega}'$, and that the scattering cross-section may be expanded as the following series of Legendre polynomials

$$\Sigma_s(\vec{r},\mu_0) = \sum_{l=0}^{\infty} \frac{2l+1}{4\pi} \Sigma_{sl}(\vec{r})\, P_l(\mu_0) \ . \tag{3}$$

We will use Cartesian coordinates that, for computational purposes, will be denoted consecutively, $x = x_1$, $y = x_2$, $z = x_3$, and also for intermediate calculations the following "complex" coordinates are introduced

$$x_{+1} = -\frac{1}{\sqrt{2}}(x+iy) \ , \quad x_{-1} = \frac{1}{\sqrt{2}}(x-iy) \ , \quad x_0 = z \ , \tag{4}$$

since the identity

$$\vec{\Omega}\,\vec{\nabla} = \sqrt{\frac{4\pi}{3}} \sum_{k=-1}^{+1} Y_1^k(\vec{\Omega}) \frac{\partial}{\partial x_k}$$

is satisfied. Substituting Eqs. (2) and (3) into Eq. (1) and integrating with respect to $\int d\vec{\Omega}\, Y_l^m(\vec{\Omega})^*$ results in the following equations for the spherical harmonics moments ϕ_l^m:

$$\begin{aligned} &- \frac{a^+_{+,lm}}{c_l^+} \frac{1}{\sqrt{2}} \frac{\partial \phi_{l+1}^{m-1}}{\partial x_{+1}} - \frac{a^+_{-,lm}}{c_l^+} \frac{1}{\sqrt{2}} \frac{\partial \phi_{l+1}^{m+1}}{\partial x_{-1}} + \frac{a^+_{0,lm}}{c_l^+} \frac{\partial \phi_{l+1}^{m}}{\partial x_{0}} \\ &+ \frac{a^-_{+,lm}}{c_l^-} \frac{1}{\sqrt{2}} \frac{\partial \phi_{l-1}^{m-1}}{\partial x_{+1}} + \frac{a^-_{-,lm}}{c_l^-} \frac{1}{\sqrt{2}} \frac{\partial \phi_{l-1}^{m+1}}{\partial x_{-1}} + \frac{a^-_{0,lm}}{c_l^-} \frac{\partial \phi_{l-1}^{m}}{\partial x_{0}} + \Sigma_t \phi_l^m \\ &\quad = \Sigma_{sl} \phi_l^m + \delta_{l0}\delta_{m0} \frac{1}{\lambda} \nu\Sigma_f \phi_0^0 \ , \qquad l = 0,1,\dots \ , \ m = -l,\dots,+l \ , \end{aligned} \tag{5}$$

where δ_{0l} is the Kronecker delta and the following constants have been introduced

$$
\begin{aligned}
a^+_{-,lm} &= [(l+m+2)(l+m+1)]^{1/2}\,, & a^+_{0,lm} &= [(l+m+1)(l-m+1)]^{1/2},\\
a^-_{-,lm} &= [(l-m)(l-m-1)]^{1/2}\,, & a^-_{0,lm} &= [(l+m)(l-m)]^{1/2},\\
a^\pm_{+,lm} &= a^\pm_{-,l\,-m}\ , & c^+_l &= [(2l+3)(2l+1)]^{1/2},\ c^-_l = c^+_{l-1}\ .
\end{aligned}
$$

In these equations it is understood that terms involving moments ϕ^m_l with invalid indices l and m are zero.

To obtain a finite approximation, the series in expansions (2) and (3) are truncated at some finite order $l = L$ and the resulting Eqs. (5) are known as the P_L equations. In the following, we will only consider L to be an odd integer.

From the index structure of Eqs. (5) we observe that it is convenient to gather even l moments into vector $X = (\phi^m_l)_{l=\text{even}}$, with $n_e = L(L+1)/2$ components, and odd l moments into vector $\bar{X} = (\phi^m_l)_{l=\text{odd}}$, with $n_o = (L+1)(L+2)/2$ components (for example, if $L = 1$ then $X = (\phi^0_0)$ and $\bar{X} = (\phi^{-1}_1, \phi^0_1, \phi^1_1)^T$). Then Eqs. (5) can be rewritten as

$$
\sum_{j=1}^{3} M_j \frac{\partial \bar{X}}{\partial x_j} + \text{diag}(\Sigma_t - \Sigma_{sl})_{l=\text{even}} X = \frac{1}{\lambda}\,\text{diag}(\delta_{l0}\,\nu\Sigma_f)_{l=\text{even}} X\ , \tag{6}
$$

$$
\sum_{j=1}^{3} \bar{M}_j \frac{\partial X}{\partial x_j} + \text{diag}(\Sigma_t - \Sigma_{sl})_{l=\text{odd}} \bar{X} = 0\ , \tag{7}
$$

where Cartesian coordinates x_j, $j = 1, 2, 3$, have been recovered and M_j and $\bar{M}_j$ are rectangular matrices (of dimension $n_e \times n_o$ and $n_o \times n_e$, respectively) defined from the coefficients of Eqs. (5). Clearly, Eq. (7) relates $\bar{X}$ with derivatives of X so it corresponds to a generalization of "Fick's law":

$$
\bar{X} = -D \sum_{j=1}^{3} \bar{M}_j \frac{\partial X}{\partial x_j}\ , \tag{8}
$$

where $D = \text{diag}(\Sigma_t - \Sigma_{sl})^{-1}_{l=\text{odd}}$ is a square matrix. Replacing Eq. (8) into Eq. (6) we obtain the "diffusive form of P_L equations"

$$
-\sum_{i,j=1}^{3} \frac{\partial}{\partial x_i}\left(M_i D \bar{M}_j \frac{\partial X}{\partial x_j} \right) + \text{diag}(\Sigma_t - \Sigma_{sl})_{l=\text{even}} X = \frac{1}{\lambda}\,\text{diag}(\delta_{l0}\,\nu\Sigma_f)_{l=\text{even}} X\ . \tag{9}
$$

The (square) "effective diffusion matrices" $M_i D \bar{M}_j$ generalize the diffusion coefficient $1/(3(\Sigma_t - \Sigma_{s1}))$ of P_1 equation to P_L equations for $L > 1$. Notice that vector $\bar{X}$ enters into the "diffusive P_L equations" (8) through the combination $M_i \bar{X}$, where the index i corresponds to each spatial direction.

We observe that Eq. (9) is complex, but the angular neutronic flux, $\Phi(\vec{r},\vec{\Omega})$, must be a real function. This implies that the complex moments satisfy the relation $\phi_l^{m*} = (-1)^m \phi_l^{-m}$. Introducing the real moments, defined as

$$\xi_l^m = \text{Re }(\phi_l^m) = \frac{1}{2}(\phi_l^m + (-1)^m \phi_l^{-m}) \,, \quad \eta_l^m = \text{Im }(\phi_l^m) = \frac{1}{2i}(\phi_l^m - (-1)^m \phi_l^{-m}) \,, \tag{10}$$

the corresponding real vectors $X = (\xi_l^m, \eta_l^m)_{l=\text{even}}$ and $\bar{X} = (\xi_l^m, \eta_l^m)_{l=\text{odd}}$ are defined and the real form of the "diffusive P_L equations" (9) can be easily obtained.

Finally, Eq. (9) corresponds to 3D geometry. Lower dimensional geometries are obtained by imposing restrictions to the angular neutronic flux. The XY (2D) geometry is obtained by imposing that the angular neutronic flux does not depend on the third coordinate, $\Phi = \Phi(x, y, \vec{\Omega})$, so $\frac{\partial \Phi}{\partial z} = 0$, and also must obey the symmetry relation $\Phi(\theta) = \Phi(\pi - \theta)$, so the moments $\phi_l^m = 0$ if $l + m$ is odd (see the subsection on reflecting boundary conditions). The planar (1D) geometry is obtained imposing that the neutronic flux $\Phi = \Phi(z, \theta)$ so the only nonzero moments are $\phi_l^{m=0}$.

2.1 Vacuum boundary conditions

When the region described by Eq. (1) is surrounded by vacuum, the angular neutronic flux at external surfaces is zero for every incoming direction,

$$\Phi(\vec{r},\vec{\Omega}) = 0 \,, \qquad \text{for all } \vec{\Omega}\,\vec{n} \leq 0 \,, \tag{11}$$

where $\vec{n}$ is the outwardly directed unitary normal vector to the external surface. This condition can be approximated by setting Marshak's conditions (Stacey, 2001)

$$\int_{\vec{\Omega}\,\vec{n}\leq 0} d\vec{\Omega}\; Y_l^m(\vec{\Omega})^*\, \Phi(\vec{r},\vec{\Omega}) = 0 \,, \tag{12}$$

for $l = 1, 3, 5, \ldots, L$ (odd) and $m = 0, 1, \ldots, l$ (the conditions with negative m index are redundant because the neutronic flux Φ is a real function). We will only consider regions with prismatic geometry; we can then use the symmetry $Y_l^m(-\vec{\Omega}) = (-1)^l Y_l^m(\vec{\Omega})$ and obtain that

$$\int_{\vec{\Omega}\,\vec{n}\leq 0} d\vec{\Omega}\; Y_l^m(\vec{\Omega})^*\, Y_{l'}^{m'}(\vec{\Omega}) = \frac{1}{2}\int d\vec{\Omega}\; Y_l^m(\vec{\Omega})^*\, Y_{l'}^{m'}(\vec{\Omega}) = \frac{1}{2}\delta_{ll'}\delta_{mm'} \,, \text{ for } l + l' \text{ even.} \tag{13}$$

Inserting the expansion given by Eq. (2), truncated up to a finite order L odd, into Marshak's conditions (12) and using (13), results into the conditions

$$\frac{1}{2}\phi_l^m + \sum_{l' \text{ even}}^{L-1} \sum_{m'=-l'}^{l'} \left(\int_{\vec{\Omega}\,\vec{n}\leq 0} d\vec{\Omega}\; Y_l^m(\vec{\Omega})^*\, Y_{l'}^{m'}(\vec{\Omega}) \right) \phi_{l'}^{m'} = 0 \,, \tag{14}$$

for $l = 1, 3, 5, \ldots, L$, $m = 0, 1, \ldots, l$. That is, if we make use of vectors X and $\bar{X}$ defined in previous section, Marshak's conditions can be written as

$$\bar{X} + N^V X = 0 \ , \tag{15}$$

where N^V is a rectangular matrix (of dimensions $n_o \times n_e$) whose matrix elements are

$$(N^V)_{(lm),(l'm')} = 2 \int_{\vec{\Omega}\,\vec{n}\leq 0} d\vec{\Omega}\ Y_l^m(\vec{\Omega})^*\, Y_{l'}^{m'}(\vec{\Omega}) \ ,$$

where (l, m), l odd, are row indices and (l', m'), l' even, are column indices (with appropriate ordering). The numerical form of this matrix will depend on the geometry of the boundary surface, that is, the spatial axis normal to the boundary surface. For example, if the unitary normal vector $\vec{n}$ to the boundary surface points to negative Z axis, matrix N^V in Eq. (15) will be denoted as N_3^{V-} and will have components

$$\begin{aligned}(N_3^{V-})_{(lm),(l'm')} &= 2 \int_0^{2\pi} d\varphi \int_0^{\pi/2} \sin\theta d\theta\ Y_l^m(\vec{\Omega})^*\, Y_{l'}^{m'}(\vec{\Omega}) \\ &= 4\pi \delta_{mm'} H_l^m H_{l'}^m \int_0^1 d\mu\, P_l^m(\mu) P_{l'}^m(\mu) \ , \end{aligned} \tag{16}$$

where $\mu = \cos\theta$, $H_l^m = \sqrt{\frac{2l+1}{4\pi}\frac{(l-m)!}{(l+m)!}}$ and $P_l^m(\mu)$ are the associated Legendre polynomials. If vector $\vec{n}$ points to positive Z axis, the corresponding matrix $N_3^{V+} = -N_3^{V-}$ has opposite sign. Similar computations can be carried out for X and Y axis and the matrices $N_1^{V\pm}$, $N_2^{V\pm}$.

We finally observe that Marshak's conditions (12) depend on the order L of the angular approximation (see equation (14)). Also, the system of equations (15) is overdetermined because the number of equations is equal to n_o, the length of vector $\bar{X}$; as we will see in the next section, the insertion into the "diffusive P_L equations" (9) will reduce, in a canonical way, the number of conditions to be equal to n_e, the length of vector X.

2.2 Reflecting boundary conditions

Reflecting boundary conditions are applied at planes of symmetry. If physical conditions are equal at both sides, the neutronic flux must satisfy, at the symmetry plane,

$$\Phi(\vec{r}, \vec{\Omega}) = \Phi(\vec{r}, \vec{\tilde{\Omega}}) \ , \tag{17}$$

where $\vec{\tilde{\Omega}}$ is the reflected angular direction with respect to the symmetry plane. For example, if the normal vector $\vec{n}$ to the symmetry plane points to the negative Z axis, the symmetry condition is

$$\Phi(\vec{r}, \varphi, \theta) = \Phi(\vec{r}, \varphi, \pi - \theta) \ , \quad \text{for } 0 < \varphi < 2\pi \, , \ 0 < \theta < \pi/2 \ . \tag{18}$$

Inserting expansion (2), this equation is equivalent to the following

$$\sum_{l=0}^{\infty} \sum_{m=-l}^{+l} (1 - (-1)^{l+m})\, \phi_l^m(\vec{r})\, Y_l^m(\vec{\Omega}) = 0 \ ,$$

that is,

$$\phi_l^m = 0 \ , \qquad \text{whenever } l + m \text{ odd}, \tag{19}$$

for $l = 0, 1, \ldots,$ $m = 0, 1, \ldots, l$. Notice that this condition is the same for normal vector $\vec{n}$ pointing to the positive Z axis. It also corresponds to the XY symmetry for 2D geometry. In the particular case of 1D geometry, only $m = 0$ moments are nonzero so the symmetry condition is $\phi_l^0 = 0$ for l odd.

If the spherical harmonics expansion (2) is truncated at finite order L then equations (19) form a set of $L(L+1)/2 = n_e$ conditions. For computational purposes it is convenient to write symmetry conditions in matrix form. We will split vectors X and $\bar{X}$ in blocks that, written symbolically, are

$$X = \begin{bmatrix} \phi_{l=\text{even}}^{m=\text{even}} \\ \phi_{l=\text{even}}^{m=\text{odd}} \end{bmatrix} \ , \qquad \bar{X} = \begin{bmatrix} \phi_{l=\text{odd}}^{m=\text{even}} \\ \phi_{l=\text{odd}}^{m=\text{odd}} \end{bmatrix} \ . \tag{20}$$

Then symmetry conditions (19) are equivalent to

$$N_3^R X = 0 \qquad \text{and} \qquad \bar{N}_3^R \bar{X} = 0 \ , \tag{21}$$

at the symmetry surface, where N_3^R is a square matrix of dimension $n_e \times n_e$ and $\bar{N}_3^R$ is a rectangular matrix of dimension $n_e \times n_o$ with the following block structure ($\mathbb{I}$ is the identity matrix)

$$N_3^R = \begin{bmatrix} 0 & 0 \\ 0 & \mathbb{I} \end{bmatrix} \ , \qquad \bar{N}_3^R = \begin{bmatrix} \mathbb{I} & 0 \\ 0 & 0 \end{bmatrix} \ .$$

In a similar fashion, reflective boundary conditions are computed when the normal vector to the symmetry surface points to X and Y axis and are the following

$$\phi_l^m - (-1)^m \phi_l^{m*} = 0 \ , \qquad \text{for YZ symmetry surface,} \tag{22}$$

$$\phi_l^m - \phi_l^{m*} = 0 \ , \qquad \text{for XZ symmetry surface.} \tag{23}$$

Finally, matrices N_j^R and $\bar{N}_j^R$, $j = 1, 2$, can be defined as before.

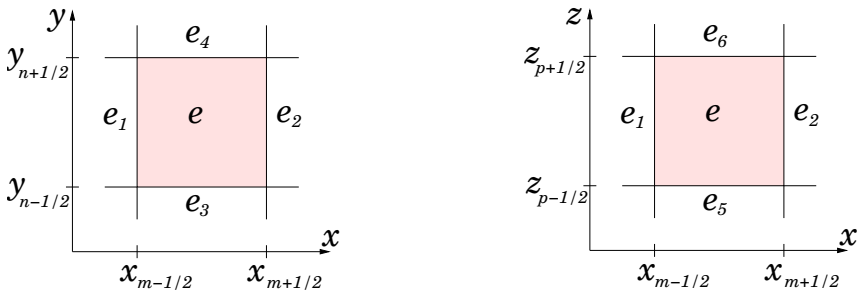

Fig. 1. Position of the neighbouring elements of node e.

3 The nodal collocation method

Since P_L equations (9) have a diffusive form, their spatial discretization can be done using a nodal collocation method, previously used for the neutron diffusion equation (Hébert, 1987; Verdú et al., 1994) and generalized for multidimensional rectangular geometries in Capilla et al. (2005). We will briefly describe the method.

The first step to discretize the P_L equations is to divide the region where these equations have to be solved into N prismatic nodes of the form

$$\mathcal{N}^e = \prod_{j=1}^{3} [x_{j,m-\frac{1}{2}}, x_{j,m+\frac{1}{2}}] \ .$$

In Fig. 1, a scheme of the discretization for a generic node e and the convention used to label the six neighbouring elements that share a surface with element e is shown. For a generic node e the change of variables

$$u_j = \frac{1}{\Delta x_j^e} \Big(x_j - \frac{1}{2}(x_{j,m-\frac{1}{2}} + x_{j,m+\frac{1}{2}}) \Big) \ , \tag{24}$$

where $\Delta x_j^e = x_{j,m+\frac{1}{2}} - x_{j,m-\frac{1}{2}}$, $j = 1, 2, 3$ transforms the node e into the cube of volume one, $\mathcal{N}_u^e = \left[-\frac{1}{2}, +\frac{1}{2}\right]^3$.

The nodal collocation method assumes that on each node the nuclear cross-sections are constant. For each node e, Eqs. (9) are transformed by means of the change of variables (24). Furthermore, if $X^e(u_1, u_2, u_3)$ denotes the previously defined vector of l even moments that appear in Eqs. (9), it is assumed that vector X^e can be expanded in terms of (orthonormal) Legendre polynomials $\mathcal{P}_k(u)$ (Capilla et al., 2005) up to a certain finite order M,

$$X^e(u_1, u_2, u_3) = \sum_{k_1,k_2,k_3=0}^{M} x^e_{k_1 k_2 k_3} \mathcal{P}_{k_1}(u_1)\, \mathcal{P}_{k_2}(u_2)\, \mathcal{P}_{k_2}(u_3) \,, \quad u_j \in [-\frac{1}{2}, \frac{1}{2}] \,. \tag{25}$$

The series (25) is then inserted into Eqs. (9) and equations for the Legendre

moments $x^e_{k_1k_2k_3}$ are derived multiplying by the weight function

$$W_{r_1r_2r_3} = \mathcal{P}_{r_1}(u_1)\,\mathcal{P}_{r_2}(u_2)\,\mathcal{P}_{r_3}(u_3)\,, \quad r_1, r_2, r_3 = 0, 1, \ldots, M\ ,$$

and integrating over the cube $\mathcal{N}^e_u$.

In performing this process, integration of "diagonal terms" in Eqs. (9), that is, $\mathrm{diag}(\Sigma_t - \Sigma_{sl})_{l=\mathrm{even}} X^e$ and $\frac{1}{\lambda}\,\mathrm{diag}(\delta_{l0}\,\nu\Sigma_f)_{l=\mathrm{even}} X^e$, is straightforward using the orthonormality properties of $\mathcal{P}_k(u)$.

Integration of second derivative terms for node e,

$$-M_i D^e \bar{M}_j \,\frac{1}{\Delta x^e_i \Delta x^e_j}\frac{\partial^2 X^e}{\partial u_i u_j}(u_1, u_2, u_3)\ , \qquad i, j = 1, 2, 3\ , \tag{26}$$

will be different when $i \neq j$ or when $i = j$. The "effective diffusion matrices" $M_i D^e \bar{M}_j$ for node e and directions i, j are not affected by integration and, for convenience, will be ommited from the next calculations. If indices are diferent, $i \neq j$, integration is straightforward using the following identity

$$\int_{-\frac{1}{2}}^{+\frac{1}{2}} du\,\mathcal{P}_r(u)\,\mathcal{P}'_k(u) = \begin{cases} 0\ , & k < r+1\ , \\ \sqrt{2r+1}\sqrt{2k+1}\,(1-(-1)^{r+k})\ , & k \geq r+1\ . \end{cases} \tag{27}$$

For example, cross-derivatives along the XY directions results into the term

$$F^e_{12;r_1r_2r_3} = -\frac{1}{\Delta x^e_1 \Delta x^e_2}\sum_{k_1,k_2=0}^{M}\Big[\int_{-\frac{1}{2}}^{+\frac{1}{2}} du_1\,\mathcal{P}_{r_1}(u_1)\,\mathcal{P}'_{k_1}(u_1)\Big]$$
$$\times\Big[\int_{-\frac{1}{2}}^{+\frac{1}{2}} du_2\,\mathcal{P}_{r_2}(u_2)\,\mathcal{P}'_{k_2}(u_2)\Big]\,x^e_{k_1k_2r_3} = \frac{1}{\Delta x^e_1 \Delta x^e_2}\sum_{\substack{k_1=r_1+1\\k_2=r_2+1}}^{M-1} A^e_{12;r_1k_1,r_2k_2}\,x^e_{k_1k_2r_3}\ , \tag{28}$$

where

$$A^e_{12;r_1k_1,r_2k_2} = -\sqrt{2r_1+1}\sqrt{2k_1+1}\,(1-(-1)^{r_1+k_1})$$
$$\times\sqrt{2r_2+1}\sqrt{2k_2+1}\,(1-(-1)^{r_2+k_2})\ . \tag{29}$$

Double derivative terms in Eqs. (26) will involve, as we will see, coupling with neighbouring nodes. To illustrate this point, let us consider the second derivative term along the X direction. Using the identity (A.7) of Capilla et al. (2005), it can be written as

$$F^e_{11;r_1r_2r_3} = -\frac{1}{(\Delta x^e_1)^2}\int_{-\frac{1}{2}}^{+\frac{1}{2}} du_1\,\mathcal{P}_{r_1}(u_1)\,\frac{d^2 X^e_{r_2r_3}}{du_1^2}(u_1)$$

$$= -\frac{1}{(\Delta x_1^e)^2}\left[\mathcal{P}_{r_1}(u_1)\frac{dX^e_{r_2r_3}}{du_1}(u_1) - \mathcal{P}'_{r_1}(u_1)X^e_{r_2r_3}(u_1)\right]_{-\frac{1}{2}}^{+\frac{1}{2}}$$
$$- \frac{1}{(\Delta x_1^e)^2}\sum_{\substack{k=0\\ r_1\geq 2}}^{r_1-2} x^e_{kr_2r_3}\int_{-\frac{1}{2}}^{+\frac{1}{2}} du_1 \mathcal{P}_k(u_1)\mathcal{P}''_{r_1}(u_1)\ , \quad (30)$$

where $X^e_{r_2r_3}(u_1)$ are the (Legendre) moments for fixed u_1 coordinate,

$$X^e_{k_2k_3}(u_1) = \int_{-\frac{1}{2}}^{\frac{1}{2}} du_2 \int_{-\frac{1}{2}}^{\frac{1}{2}} du_3 \mathcal{P}_{k_2}(u_2)\mathcal{P}_{k_3}(u_3)X^e(u_1,u_2,u_3)$$
$$= \sum_{k_1=0}^{M} x^e_{k_1k_2k_3}\,\mathcal{P}_{k_1}(u_1)\ . \quad (31)$$

From Eq. (30) we observe that we need to evaluate $X^e_{r_2r_3}$ and $\frac{dX^e_{r_2r_3}}{du_1}$ at boundaries $u_1 = \pm\frac{1}{2}$. Let us first consider the case when node e is an interior node and the boundary between two adjacent nodes falls in the YZ plane, with normal vector to the surface pointing to the negative X axis. Then we will consider the interface between node e and node e_1, see Fig. 1. Adjacent nodes are then related imposing continuity of the angular flux $\Phi(\vec{r},\vec{\Omega})$ at the boundary. This implies continuity of all moments in Eq. (2) at the interface surface

$$\phi_l^{m,e}\left(-\frac{1}{2},u_2,u_3\right) = \phi_l^{m,e_1}\left(+\frac{1}{2},u_2,u_3\right)\ , \qquad l=0,1,\ldots,L\ ,$$

and, equivalently, splitting moments of even and odd l, continuity conditions for vectors X^e and $\bar{X}^e$ at node e,

$$X^e\left(-\frac{1}{2},u_2,u_3\right) = X^{e_1}\left(+\frac{1}{2},u_2,u_3\right)\ , \quad (32)$$
$$-\sum_{j=1}^{3}\frac{D^e\bar{M}_j}{\Delta x_j^e}\frac{\partial X^e}{\partial u_j}\left(-\frac{1}{2},u_2,u_3\right) = -\sum_{j=1}^{3}\frac{D^{e_1}\bar{M}_j}{\Delta x_j^{e_1}}\frac{\partial X^{e_1}}{\partial u_j}\left(+\frac{1}{2},u_2,u_3\right)\ , \quad (33)$$

where in last line Eq. (8) ("Fick's law") has been used to write $\bar{X}$ in terms of X. Notice that the continuity condition given by Eq. (33) will involve normal and tangent derivatives of vector $\bar{X}$ at the boundary surface. Observe also that $\Delta x_2^e = \Delta x_2^{e_1}$ and $\Delta x_3^e = \Delta x_3^{e_1}$ because the interface surface falls in the YZ plane. Also Eq. (33) implies continuity of tangent derivatives along the YZ plane,

$$\frac{\partial X^e}{\partial u_j}\left(-\frac{1}{2},u_2,u_3\right) = \frac{\partial X^{e_1}}{\partial u_j}\left(-\frac{1}{2},u_2,u_3\right)\ , \qquad j=2,3\ .$$

We modify Eq. (33) to take into account these conditions and also the fact that Eq. (30) must be premultiplied by the "effective diffusion matrices", as

appear in Eq. (26). So we obtain

$$\frac{M_1 D^e \bar{M}_1}{\Delta x_1^e}\frac{\partial X^e}{\partial u_1}\left(-\frac{1}{2},u_2,u_3\right) = \frac{M_1 D^{e_1} \bar{M}_1}{\Delta x_1^{e_1}}\frac{\partial X^{e_1}}{\partial u_1}\left(+\frac{1}{2},u_2,u_3\right) - \sum_{j=2}^{3}\frac{M_1(D^e - D^{e_1})\bar{M}_j}{\Delta x_j^e}\frac{\partial X^e}{\partial u_j}\left(-\frac{1}{2},u_2,u_3\right) \ . \quad (34)$$

If we integrate Eqs. (32) and Eq. (34) with respect to $\int_{-\frac{1}{2}}^{+\frac{1}{2}} du_2 \int_{-\frac{1}{2}}^{+\frac{1}{2}} du_3\, \mathcal{P}_{r_2}(u_2)\,\mathcal{P}_{r_3}(u_3)$, there result equivalent continuity conditions for the moments $X^e_{r_2 r_3}(u_1)$ defined in Eq. (31) and their derivatives

$$X^e_{r_2 r_3}\left(-\frac{1}{2}\right) = X^{e_1}_{r_2 r_3}\left(+\frac{1}{2}\right) \ , \quad (35)$$

$$\frac{M_1 D^e \bar{M}_1}{\Delta x_1^e}\frac{\partial X^e_{r_1 r_2}}{\partial u_1}\left(-\frac{1}{2}\right) = \frac{M_1 D^{e_1} \bar{M}_1}{\Delta x_1^{e_1}}\frac{\partial X^{e_1}_{r_2 r_3}}{\partial u_1}\left(+\frac{1}{2}\right) - \sum_{j=2}^{3}\frac{M_1(D^e - D^{e_1})\bar{M}_j}{\Delta x_j^e}\int_{-\frac{1}{2}}^{+\frac{1}{2}} du_2 \int_{-\frac{1}{2}}^{+\frac{1}{2}} du_3\, \mathcal{P}_{r_2}(u_2)\,\mathcal{P}_{r_3}(u_3)\frac{\partial X^e}{\partial u_j}\left(-\frac{1}{2},u_2,u_3\right) \ . \quad (36)$$

Finally, Eqs (35), (36) and the identities (A.8) and (A.9) of Capilla et al. (2005) give the needed expressions for vector $X^e_{r_2 r_3}$ and their derivative

$$X^e_{r_2 r_3}\left(-\frac{1}{2}\right) = \sum_{k_1=0}^{M-1}[(\mathbb{I} - \mathcal{W}_{11}^{e-})(-1)^{k_1} c_{k_1} x^e_{k_1 r_2 r_3} + \mathcal{W}_{11}^{e-} c_{k_1} x^{e_1}_{k_1 r_2 r_3}] + \sum_{j=2}^{3}\frac{\mathcal{W}_{1j}^{e-}}{M(M+1)}\int_{-\frac{1}{2}}^{+\frac{1}{2}} du_2 \int_{-\frac{1}{2}}^{+\frac{1}{2}} du_3\, \mathcal{P}_{r_2}(u_2)\,\mathcal{P}_{r_3}(u_3)\frac{\partial X^e}{\partial u_j}\left(-\frac{1}{2},u_2,u_3\right) \ , \quad (37)$$

$$\frac{\partial X^e_{r_2 r_3}}{\partial u_1}\left(-\frac{1}{2}\right) = M(M+1)\,\mathcal{W}_{11}^{e-}\sum_{k_1=0}^{M-1} c_{k_1}[(-1)^{k_1} x^e_{k_1 r_2 r_3} - x^{e_1}_{k_1 r_2 r_3}] - \sum_{j=2}^{3}\mathcal{W}_{1j}^{e-}\int_{-\frac{1}{2}}^{+\frac{1}{2}} du_2 \int_{-\frac{1}{2}}^{+\frac{1}{2}} du_3\, \mathcal{P}_{r_2}(u_2)\,\mathcal{P}_{r_3}(u_3)\frac{\partial X^e}{\partial u_j}\left(-\frac{1}{2},u_2,u_3\right) \ , \quad (38)$$

where $\mathbb{I}$ is the identity matrix, the coefficients $c_k = \sqrt{2k+1}\left(1 - \frac{k(k+1)}{M(M+1)}\right)$ and the "normal and tangent coupling factors" $\mathcal{W}_{ij}^{e-}$ are defined as the matrix solutions of the following systems

$$M_1\left(\frac{D^e}{\Delta x_1^e} + \frac{D^{e_1}}{\Delta x_1^{e_1}}\right)\bar{M}_1\ \mathcal{W}_{11}^{e-} = M_1\frac{D^{e_1}}{\Delta x_1^{e_1}}\bar{M}_1 \ ,$$
$$M_1\left(\frac{D^e}{\Delta x_1^e} + \frac{D^{e_1}}{\Delta x_1^{e_1}}\right)\bar{M}_1\ \mathcal{W}_{1j}^{e-} = M_1\frac{D^e - D^{e_1}}{\Delta x_j^{e_1}}\bar{M}_j \ , \qquad \text{if } j = 1,2 \ . \quad (39)$$

We notice that if scattering is isotropic then Eq. (39) simplifies to $\mathcal{W}_{11}^{e-} =$

diag $\left[\frac{D^{e_1}}{\Delta x_1^{e_1}}\left(\frac{D^e}{\Delta x_1^e}+\frac{D^{e_1}}{\Delta x_1^{e_1}}\right)^{-1}\right]$. Integrals in Eqs. (37,38) will be evaluated inserting series expansion (25) and then using the identity (27).

This procedure will be repeated when normal vector points to forward X direction. Then we will consider coupling between node e and node e_2, see Fig. 1. In an analogous way, the following expressions are obtained

$$X^e_{r_2r_3}\left(+\frac{1}{2}\right) = \sum_{k_1=0}^{M-1}[\mathcal{W}^{e+}_{11}(-1)^{k_1}c_{k_1}x^{e_2}_{k_1r_2r_3} + (\mathbb{I}-\mathcal{W}^{e+}_{11})c_{k_1}x^e_{k_1r_2r_3}] \tag{40}$$
$$-\sum_{j=2}^{3}\frac{\mathcal{W}^{e+}_{1j}}{M(M+1)}\int_{-\frac{1}{2}}^{+\frac{1}{2}}du_2\int_{-\frac{1}{2}}^{+\frac{1}{2}}du_3\,\mathcal{P}_{r_2}(u_2)\,\mathcal{P}_{r_3}(u_3)\frac{\partial X^e}{\partial u_j}\left(+\frac{1}{2},u_2,u_3\right)\ ,$$

$$\frac{\partial X^e_{r_2r_3}}{\partial u_1}\left(+\frac{1}{2}\right) = M(M+1)\,\mathcal{W}^{e+}_{11}\sum_{k_1=0}^{M-1}c_{k_1}[(-1)^{k_1}x^{e_2}_{k_1r_2r_3}-x^e_{k_1r_2r_3}] \tag{41}$$
$$-\sum_{j=2}^{3}\mathcal{W}^{e+}_{1j}\int_{-\frac{1}{2}}^{+\frac{1}{2}}du_2\int_{-\frac{1}{2}}^{+\frac{1}{2}}du_3\,\mathcal{P}_{r_2}(u_2)\,\mathcal{P}_{r_3}(u_3)\frac{\partial X^e}{\partial u_j}\left(+\frac{1}{2},u_2,u_3\right)\ ,$$

where the matrix "coupling factors" $\mathcal{W}^{e+}_{ij}$ are defined as in Eq. (39) just replacing e_1 by e_2.

From Eqs. (37, 38, 40, 41), the computation of integral (30) is the vector analogue of the procedure described in Capilla et al. (2005), and results in the expression that relates nodes e_1 and e_2 adjacent to node e along the X direction

$$F^e_{11;r_1r_2r_3} = \frac{1}{(\Delta x^e_1)^2}\Big\{\sum_{k_1=0}^{M-1}\Big[A^{ee_1}_{r_1;k_1}\,x^{e_1}_{k_1r_2r_3}+A^{ee}_{r_1;k_1}\,x^e_{k_1r_2r_3}+A^{e_2e}_{r_1;k_1}\,x^{e_2}_{k_1r_2r_3}\Big]$$
$$+\sum_{k_1=0}^{M-1}\sum_{k_2=r_2+1}^{M-1}A^{ee}_{r_1r_2;k_1k_2}\,x^e_{k_1k_2r_3}+\sum_{k_1=0}^{M-1}\sum_{k_3=r_3+1}^{M-1}A^{ee}_{r_1r_3;k_1k_3}\,x^e_{k_1r_2k_3}\Big\}\ , \tag{42}$$

where the following "matrix elements" have been defined

$$A^{ee_1}_{r;k} = -M(M+1)(-1)^r c_k\,c_r\,\mathcal{W}^{e-}_{11}\ ,$$
$$A^{ee}_{r;k} = M(M+1)\,c_k\,c_r\,[(-1)^{r+k}\mathcal{W}^{e-}_{11}+\mathcal{W}^{e+}_{11}]$$
$$+\sqrt{2r+1}\sqrt{2k+1}(1+(-1)^{r+k})\begin{cases}\left(1-\frac{r(r+1)}{M(M+1)}\right)k(k+1)\ , & k<r\ ,\\ \left(1-\frac{k(k+1)}{M(M+1)}\right)r(r+1)\ , & k\geq r\ ,\end{cases}$$
$$A^{e_2e}_{r;k} = -M(M+1)(-1)^k c_k\,c_r\,\mathcal{W}^{e+}_{11}\ ,$$
$$A^{ee}_{r_1r_j;k_1k_j} = -c_{r_1}\sqrt{2k_1+1}\sqrt{2r_j+1}\sqrt{2k_j+1}(1-(-1)^{r_j+k_j})$$
$$\times[(-1)^{r_1+k_1}\mathcal{W}^{e-}_{1j}-\mathcal{W}^{e+}_{1j}]\ ,\qquad j=2,3\ . \tag{43}$$

In the case that the node e is adjacent to the vacuum boundary as, for example,

when the vacuum boundary falls in the XY plane and the normal vector to the surface points to the negative Z axis, then Marshak vacuum boundary conditions (15) are used,

$$\bar{X}\left(u_1, u_2, -\frac{1}{2}\right) + N_3^{V-}\, X^e\left(u_1, u_2, -\frac{1}{2}\right) = 0 \ , \tag{44}$$

where the change of variable (24) has been performed. If we use Eq. (8) ("Fick's law") to replace $\bar{X}$ in terms of X and, for the same reasons commented in Eq. (33), premultiply by M_3, we obtain Marshak vacuum boundary conditions for vector X

$$-\sum_{j=1}^{3} \frac{M_3 D^e \bar{M}_j}{\Delta x_j^e} \frac{\partial X^e}{\partial u_j}\left(u_1, u_2, -\frac{1}{2}\right) + M_3 N_3^{V-}\, X^e\left(u_1, u_2, -\frac{1}{2}\right) = 0 \ . \tag{45}$$

Using again the identity (A.8) of Capilla et al. (2005) and integrating with respect to variables u_1 and u_2, there results the expressions for vector $X^e_{r_1 r_2}$

$$\begin{aligned} X^e_{r_1 r_2}\left(-\frac{1}{2}\right) &= \sum_{k_3=0}^{M-1} (\mathbb{I} - \Omega_{33}^{e-})(-1)^{k_3} c_{k_3} x^e_{r_1 r_2 k_3} \qquad (46)\\ &+ \sum_{j=1}^{2} \frac{\Omega_{3j}^{e-}}{M(M+1)} \int_{-\frac{1}{2}}^{+\frac{1}{2}} du_1 \int_{-\frac{1}{2}}^{+\frac{1}{2}} du_2\, \mathcal{P}_{r_1}(u_1)\, \mathcal{P}_{r_2}(u_2) \frac{\partial X^e}{\partial u_j}\left(u_1, u_2, -\frac{1}{2}\right) \ , \\ \frac{\partial X^e_{r_1 r_2}}{\partial u_3}\left(-\frac{1}{2}\right) &= M(M+1)\, \Omega_{33}^{e-} \sum_{k_3=0}^{M-1} c_{k_3} (-1)^{k_3} x^e_{r_1 r_2 k_3} \qquad (47)\\ &- \sum_{j=1}^{2} \Omega_{3j}^{e-} \int_{-\frac{1}{2}}^{+\frac{1}{2}} du_1 \int_{-\frac{1}{2}}^{+\frac{1}{2}} du_2\, \mathcal{P}_{r_1}(u_1)\, \mathcal{P}_{r_2}(u_2) \frac{\partial X^e}{\partial u_j}\left(u_1, u_2, -\frac{1}{2}\right) \ , \end{aligned}$$

where the matrix "vacuum coupling factors" Ω_{3j}^{e-}, $j = 1, 2, 3$, are defined as the solutions of the following systems

$$\begin{aligned} &\left(M(M+1)\, M_3 \frac{D^e}{\Delta x_3^e} \bar{M}_3 + M_3 N_3^{V-}\right) \Omega_{33}^{e-} = M_3 N_3^{V-} \ , \qquad (48)\\ &\left(M(M+1)\, M_3 \frac{D^e}{\Delta x_3^e} \bar{M}_3 + M_3 N_3^{V-}\right) \Omega_{3j}^{e-} = M(M+1)\, M_3 \frac{D^e}{\Delta x_j^e} \bar{M}_j \ , \quad j = 1, 2 \ . \end{aligned}$$

On comparing Eqs. (46) and (47) with Eqs. (37) and (38), we observe that Eq. (42) will be valid for all nodes taking into consideration that, for boundary nodes, the coupling factors are Ω_{3j}^{e-} and that there is no adjacent node in the direction of the boundary. A similar procedure is applied when the vacuum surface has normal vector pointing to the positive Z axis, and also to X axis and Y axis.

If node e is adjacent to a reflecting boundary as, for example, the XY plane, then conditions (21) are used and, in an analogous manner, it can be computed

that Eq. (42) will be valid but now with coupling factors Ω_{3j}^{e-} given by the following equations

$$\begin{aligned} \Omega_{33}^{e-} &= N_3^R \ , \\ \left(N_3^R + \bar{N}_3^R D^e \bar{M}_3\right) \Omega_{3j}^{e-} &= \frac{\Delta x_3^e}{\Delta x_j^e} \bar{N}_3^R D^e \bar{M}_j \ , \quad j = 1, 2 \ . \end{aligned} \tag{49}$$

Finally, once an appropriate ordering of the indices is chosen, the previous procedure approximates Eqs. (9) by a generalized eigenvalue problem that can be casted in the form

$$\mathcal{A}\, V = \frac{1}{\lambda} \mathcal{B}\, V \ , \tag{50}$$

where V is a real vector of components $(\xi_{l;k_1k_2k_3}^{m;e}, \eta_{l;k_1k_2k_3}^{m;e})$ and $\mathcal{A}$, $\mathcal{B}$ are matrices of dimension

$$N \times G \times N_{\text{Leg}} \times n_e \ , \tag{51}$$

where N is the number of nodes, G is the number of energy groups, $N_{\text{Leg}} = M^d$ is the number of Legendre moments, with M the order in Legendre series (25) and d the spatial dimension and finally $n_e = L(L+1)/2$ is the number of components of vector X (i.e. the number of even l moments), being L the order of the P_L approximation.

To increase numerical efficiency, a serendipity approximation can be consistently introduced in the nodal collocation method (Hébert, 1987). This approximation reduces the number of unknowns to the set $(\xi_{l;k_1k_2k_3}^{m;e}, \eta_{l;k_1k_2k_3}^{m;e})$ with indices $k_1 + k_2 + k_3 \leq M - 1$ and replaces the sums $\sum_{k_1=0}^{M-1}$, $\sum_{k_1=0}^{M-1} \sum_{k_2=r_2+1}^{M-1}$ in Eq. (28) and the sums $\sum_{k_1=r_1+1}^{M-1} \sum_{k_2=r_2+1}^{M-1}$ in Eq. (42) by the sums $\sum_{k_1=0}^{M-1-(r_2+r_3)}$, $\sum_{k_1=0}^{M-1} \sum_{k_2=r_2+1}^{M-1-(k_1+r_3)}$ and $\sum_{k_1=0}^{M-1} \sum_{k_2=r_2+1}^{M-1-(k_1+r_3)}$, respectively, for $r_1 + r_2 + r_3 \leq M - 1$. The dimension of the eigenvalue problem (50) reduces in Eq. (51) because the number of Legendre moments is now $N_{\text{Leg}} = M(M+1)(M+2)/6$ for 3D or $N_{\text{Leg}} = M(M+1)/2$ for 2D.

4 Numerical results

The nodal collocation method developed in previous sections has been implemented into the code SHNC written in FORTRAN 90, which solves the eigenvalue problem (50) for an arbitrary P_L approximation, with L odd.

To test the performance of the method we first consider homogeneous two and three-dimensional one-group and isotropic eigenvalue problems with small lenght side. We compare the results of sucessive P_L approximations computed with the SHNC code with results from the discrete-ordinates code DANTSYS (Alcouffe et al., 1995), which solves the transport problem using a fine spatial

mesh and an angular (S_N) quadrature set. In both homogeneous cases, a low order P_L, $L < 5$, angular approximation gives inaccurate results, since the homogeneous region considered has a small dimension, the angular dependence in the solution is large and it is necessary to consider a large order L to obtain results similar to the transport solution. We notice that, in the light of the terms added to the discretization of P_L equations using a nodal collocation method in Section 3, corresponding to the tangent derivatives of vector X at boundary surfaces (see Eq. (33) and the "tangent coupling factors" in Eq. (39)), we have recomputed all the numerical 2D test cases presented in Capilla et al. (2008). We have only observed differences in the homogeneous square region with length side of 2 cm, where the effects of the new terms are not negligible.

Second, we study two 3D realistic reactor problems: we present results from a set of multi-group eigenvalue (k_{eff}) neutron transport benchmark problems proposed by Takeda et al. (1988). The eigenvalues k_{eff} obtained using the nodal collocation method for the 3D benchmarks are compared with solutions from the deterministic finite element transport theory code EVENT (de Oliveira et al., 2001) reported in Ziver et al. (2005), the well-known Monte Carlo code MCNP4C (Ziver et al., 2005) and also with results from the NCRP Technical Report (Takeda and Ikeda, 1991).

4.1 Homogeneous 2D eigenvalue problem

We consider a homogeneous square region of width 2 cm and height 2 cm, with vacuum boundary conditions. The nuclear cross-sections for this problem are: $\Sigma_t = 1\,\text{cm}^{-1}$, $\Sigma_s = 0.9\,\text{cm}^{-1}$ and $\nu\Sigma_f = 0.25\,\text{cm}^{-1}$. In Table 1, we show the fundamental eigenvalue and those corresponding to the subcritical modes. We have taken a spatial discretization with 8 equal length intervals in each X, Y direction (a total of 64 square nodes) and $M = 4$, where M is the orthonormal Legendre polynomials order in Eq. (25). These results where computed without making use of the serendipity approximation because the problem size is small. Also we compare the first eigenvalue obtained using the successive P_L approximations with a reference solution from the discrete-ordinates TWODANT code (Alcouffe et al., 1995) using the S_{16} quadrature set, with 150×150 spatial mesh and a convergence criterion of `epsi`$=10^{-7}$. We observe convergence of the k_{eff} eigenvalue to the reference solution, as L grows.

In Fig. 2 we compare the scalar flux, obtained with the nodal collocation method (SHNC), for sucessive P_L approximations, and polynomial order $M = 4$, along the horizontal line $y = 1$ cm. In all the calculations, the normalization

Table 1
Four dominant eigenvalues for the homogeneous 2D one-group eigenvalue problem, calculated with $M = 4$

Eigenvalue	P_1	P_3	P_5	P_7	P_9	P_{11}	S_{16}
k_{eff}	0.33274	0.38301	0.38761	0.38864	0.38900	0.38919	0.38914
2nd	0.12488	0.17583	0.18755	0.18999	0.19066	0.19088	
3rd	0.12488	0.17583	0.18755	0.18999	0.19066	0.19088	
4th	0.07686	0.11334	0.12770	0.13203	0.13328	0.13377	

condition is:

$$\frac{1}{V_{\text{core}}} \sum_{e=1}^{N} \sum_{g=1}^{G} |\phi^0_{0,eg}| \, \nu\Sigma_{f,eg} \, \Delta V_e = 1 \ ,$$

where V_{core} is the core area, N is the number of nodes ($N = N_x \times N_y$), G is the number of energy groups and $\Delta V_e = \Delta x_e \, \Delta y_e$ for node e.

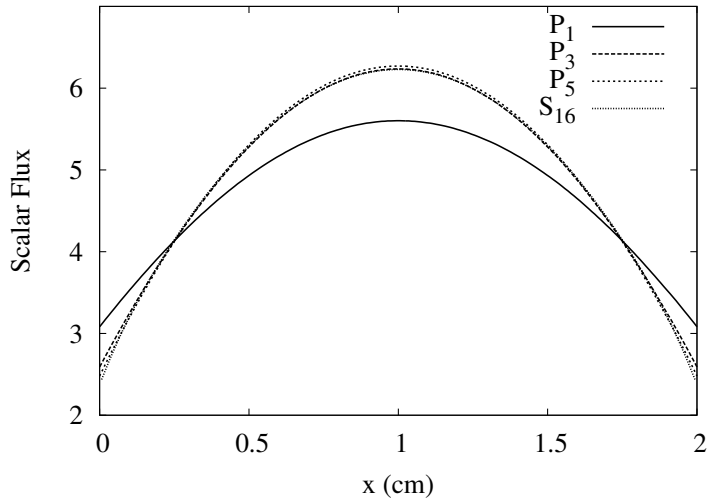

Fig. 2. Scalar flux along $y = 1$ cm of the SHNC P_L, $L = 1, 3, 5$ solutions with $M = 4$, and S_{16} reference solution for the 2D homogeneous eigenvalue problem.

4.2 Homogeneous 3D eigenvalue problem

We consider a homogeneous cubic region of side 2 cm, with vacuum boundary conditions. The nuclear cross-sections for this problem are the same as in previous subsection.

In Table 2, we show the fundamental eigenvalue and those corresponding to the subcritical modes. In this case, we have taken 4 mesh intervals in each X, Y and Z direction, resulting in a total of $4^3 = 64$ cubic nodes. Also we consider

$M = 5$ as the Legendre polynomials order in Eq. (25). Also we compare the first eigenvalue obtained using the successive P_L approximations with a reference solution from the discrete-ordinates THREEDANT code (Alcouffe et al., 1995) using the S_{16} quadrature set, with $50 \times 50 \times 50$ spatial mesh and a convergence criterion of `epsi`$=10^{-10}$.

Table 2
k_{eff} and subcritical eigenvalues for the homogeneous 3D one-group problem, for $M = 5$

Eigenvalue	P_1	P_3	P_5	P_7	P_9	S_{16}
k_{eff}	0.23221	0.27844	0.28010	0.28071	0.28092	0.28069
2nd, 3rd, 4th	0.10742	0.15498	0.16400	0.16499	0.16523	
5th, 6th, 7th	0.06987	0.10728	0.11937	0.12208	0.12251	

To investigate the convergence of the nodal collocation method for this problem, we have calculated the fundamental (k_{eff}) eigenvalue for different values of $N_x = N_y = N_z$, where N_x, N_y, N_z are the total number of meshes in X, Y and Z directions respectively. Also different values of M are considered, for the successive P_L approximations. The obtained results are shown in Table 3. Also, the serendipity approximation has not been used to perform these calculations.

Table 3
Eigenvalue k_{eff} of P_L equations for a homogeneous cubic region, computed for several values of $N_x = N_y = N_z$ and M

N_x	M	P_1	P_3	P_5	P_7	P_9
1	3	0.23241	0.28207	0.28378	0.28414	0.28429
1	4	0.23221	0.27982	0.28208	0.28257	0.28281
1	5	0.23221	0.27835	0.28000	0.28052	0.28076
2	3	0.23221	0.28103	0.28268	0.28330	0.28361
2	4	0.23221	0.27831	0.28027	0.28073	0.28112
2	5	0.23221	0.27851	0.28022	0.28083	0.28113
4	3	0.23221	0.27983	0.28207	0.28279	0.28312
4	4	0.23221	0.27840	0.28000	0.28050	0.28074
4	5	0.23221	0.27844	0.28010	0.28071	0.28092

4.3 Modelled 3D benchmark problems

In this Section, we present results from a set of multi-group eigenvalue (k_{eff}) benchmark problems in three-dimensional reactor core configurations. The principal aim is to test the capability of the nodal collocation method to treat 3D realistic reactor problems. We consider the 3D benchmark problems proposed by Takeda et al. (1988) as part of the reactor physics benchmark problems compiled and published by Nuclear Energy Agency committe on Reactor Physics Benchmarks (NEACRP). A number of cases have been studied for each benchmark problem. The specifications of geometrical structure, dimensions and materials present are briefly described here. We refer to Takeda and Ikeda (1991) for another input data such as the multi-group cross-sections and fission spectrum.

4.3.1 Benchmark problem 1

The first benchmark problem represents a small core model of a Light Water Reactor (LWR). The material cross-sections were modelled in two energy groups, representing the fast and thermal groups, respectively. The overall dimensions are $50 \times 50 \times 50$ cm. The reactor configuration is composed of a fuel region with dimensions $30 \times 30 \times 30$ cm, a void (control rods) region of $5 \times 10 \times 50$ cm, and a reflector region with $5 \times 10 \times 50$ cm, as can be seen in Fig. 3.

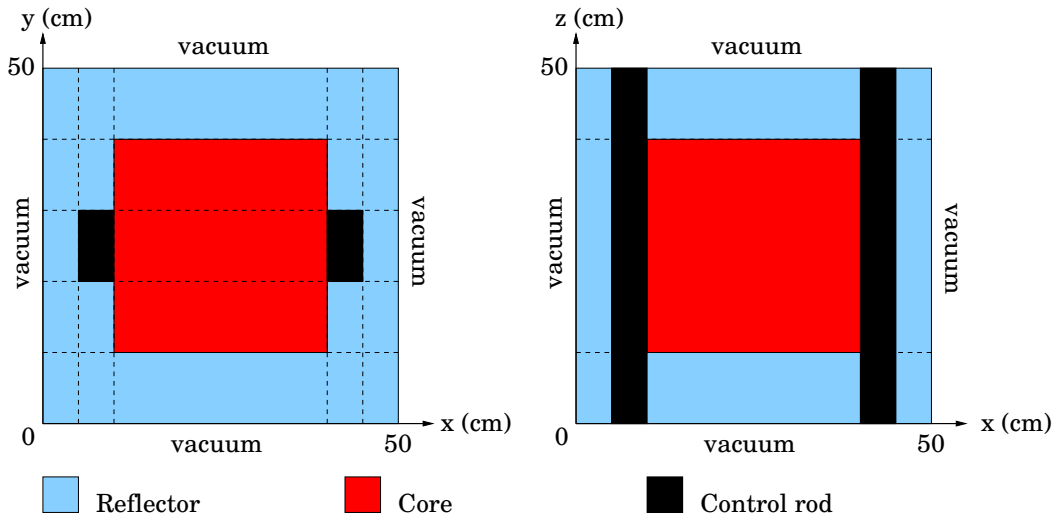

Fig. 3. Configuration of 3D benchmark problem 1. Dashed lines correspond to the spatial discretization according with the material zones.

For this Benchmark problem 1, two scenarios have been studied: Case 1) with the control rods 'in'; and Case 2) control rods 'out'. We have applied the

serendipity approximation in all the calculations performed with the nodal collocation method.

We have performed a coarse mesh calculation using a spatial discretization along each direction according with the material zones (see dashed lines in Fig. 3), and also a fine mesh calculation with mesh intervals of 5 cm. Table 4 presents the k_{eff} solutions for the coarse mesh computations using the nodal collocation method (SHNC). Solutions are presented for P_1 diffusion theory and $P_3 - P_7$ transport theory approximation. Different order (M) of orthonormal Legendre polynomials in the expansion of the fields are used. The XYZ cartesian geometry of the reactor was considered, being the number of meshes 5, 5 and 3 in X, Y and Z directions, respectively, and the total number of 3D nodes is 75. The k_{eff} eigenvalues are compared for each case to the solutions provided by the code EVENT (Ziver et al., 2005).

Table 4
Coarse mesh solutions for k_{eff} eigenvalue, using different order M and P_L approximations, for the benchmark problem 1, Case 1

Method	SHNC			EVENT
M	4	5	6	
P_1	0.92399	0.92732	0.92838	0.92874
P_3	0.96370	0.97108	0.97210	0.97245
P_5	0.96663	0.97352	0.97475	0.97555
P_7	0.96691	0.97424	0.97519	0.97641

Table 5 shows the fine mesh SHNC solutions for k_{eff} eigenvalues using different P_L approximations and values of $M = 3, 4, 5$. In these computations, with a mesh size of 5 cm, the number of meshes in X, Y and Z directions are 10, resulting in 1000 cubic nodes in 3D. The fine mesh results for the k_{eff} eigenvalue show better agreement with the EVENT results. Notice that in the reference report (Takeda and Ikeda, 1991) it is commented that, for S_N methods, the angular quadrature effect and the spatial mesh effect are relatively large. The reason for this is that a fine mesh calculation is necessary to treat the flux depression around the control rod, as seen in Fig. 5. A reference mesh size of 1 cm was then suggested. We observe that one advantage of the nodal collocation method is that it does not require a small mesh size to obtain satisfactory results.

In Figs. 4 and 5 we compare the two-group scalar fluxes along the x-axis from core centre for sucessive SHNC P_L approximations. Fig. 4 corresponds to the coarse mesh solution with polynomial order $M = 6$ and Fig. 5 corresponds to the fine mesh of 5 cm with $M = 5$.

Table 5
Fine mesh solutions for k_{eff} eigenvalue, using $M = 3, 4, 5$ and different P_L approximations, for the benchmark problem 1, Case 1

Method	SHNC			EVENT
M	3	4	5	
P_1	0.92908	0.92895	0.92878	0.92874
P_3	0.97109	0.97224	0.97312	0.97245
P_5	0.97330	0.97601	0.97586	0.97555
P_7	0.97345	0.97629	0.97670	0.97641

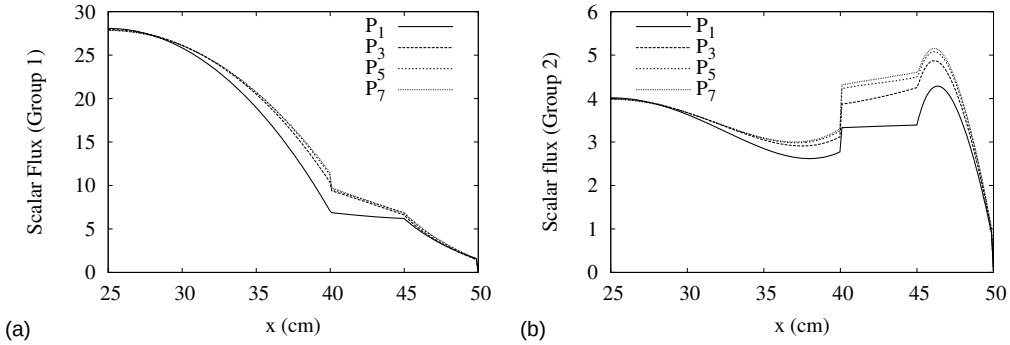

Fig. 4. Comparison of scalar flux of SHNC $P_1 - P_7$, $M = 6$, coarse mesh solutions for control rod-out (Case 1) of benchmark problem 1 from core centre of coordinates (25,25,25) to (50,25,25). (a) Energy group 1. (b) Energy group 2.

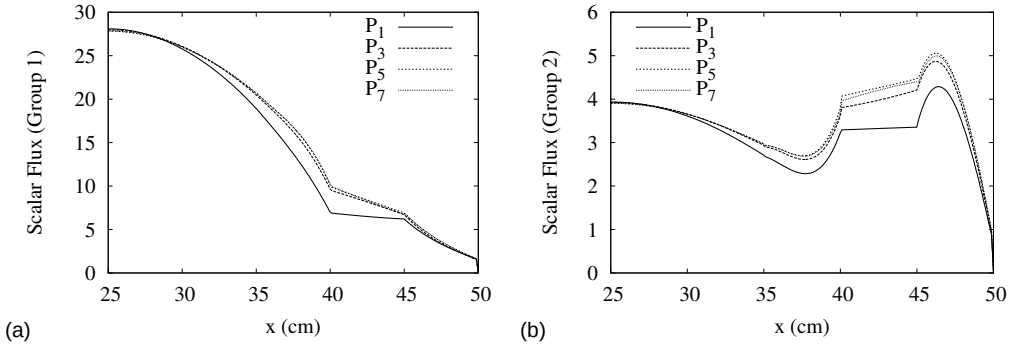

Fig. 5. Comparison of scalar flux of SHNC $P_1 - P_7$, $M = 5$, fine mesh solutions for control rod-out (Case 1) of benchmark problem 1, from core centre of coordinates (25,25,25) to (50,25,25). (a) Energy group 1. (b) Energy group 2.

Also, we have solved the eigenvalue problem for model 1 case 2. The results for k_{eff} eigenvalues are shown in Table 6 for the coarse mesh calculation and in Table 7 for the fine mesh calculation, for different values of M in comparison with the EVENT results.

Again, the results show, in general, good agreement with the EVENT predic-

Table 6
Coarse mesh solutions for k_{eff} eigenvalue for different P_L approximations and M, for the benchmark problem 1, Case 2

Method	SHNC			EVENT
M	4	5	6	
P_1	0.92820	0.93112	0.93202	0.93279
P_3	0.95037	0.95888	0.96012	0.96136
P_5	0.95083	0.95964	0.96080	0.96248
P_7	0.95085	0.95966	0.96080	0.96248

Table 7
Fine mesh solutions for k_{eff} eigenvalue for M =3, 4, 5 and different P_L approximations, for the benchmark problem 1, Case 2

Method	SHNC			EVENT
M	3	4	5	
P_1	0.93232	0.93245	0.93242	0.93279
P_3	0.95741	0.96013	0.96118	0.96136
P_5	0.95766	0.96115	0.96192	0.96248
P_7	0.95763	0.96133	0.96201	0.96248

tions, although we observe that the fine mesh calculations give better results for this benchmark problem 1, Case 2.

In Figs. 6 and 7 we compare the two-group scalar fluxes along the x-axis from core centre for sucessive SHNC P_L approximations. Fig. 6 corresponds to the coarse mesh solution with $M = 6$ and Fig. 7 corresponds to the fine mesh of 5 cm, with $M = 5$.

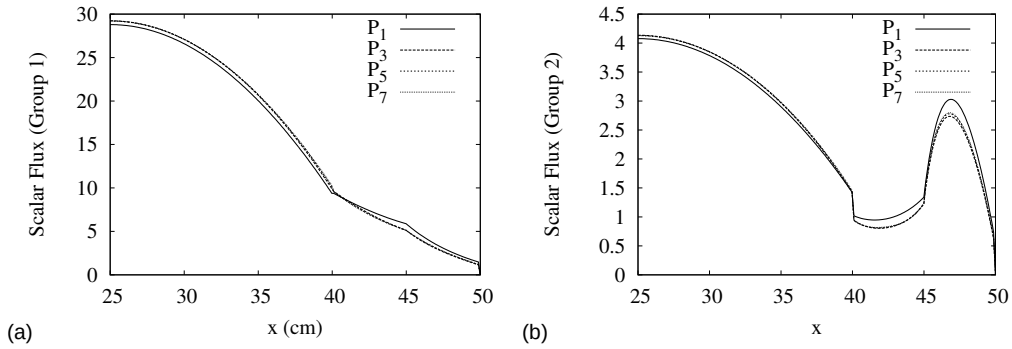

Fig. 6. Comparison of scalar flux of SHNC $P_1 - P_7$, $M = 6$, coarse mesh solutions for control rod-in (Case 2) of benchmark problem 1, from core centre of coordinates (25,25,25) to (50,25,25). (a) Energy group 1. (b) Energy group 2.

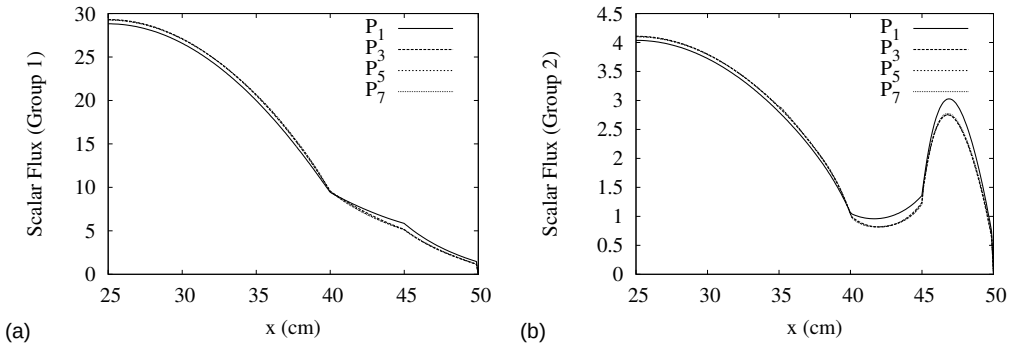

Fig. 7. Comparison of scalar flux of SHNC $P_1 - P_7$, $M = 5$, fine mesh solutions for control rod-in (Case 2) of benchmark problem 1, from core centre of coordinates (25,25,25) to (50,25,25). (a) Energy group 1. (b) Energy group 2.

In Table 8 we compare the SHNC P_L results for the k_{eff} eigenvalue against those from MCNP4C solutions reported in Ziver et al. (2005) and from the mean values and standard deviations of k_{eff} calculated by various 3D transport code methods summarized in Takeda and Ikeda (1991), for Case 1 and Case 2 problems. The differences in k_{eff} between the SHNC method and the different reported k_{eff} eigenvalues taken as reference solutions are calculated in pcm (per cent mille), $|(k_{\text{eff}}^{\text{Ref}} - k_{\text{eff}}^{\text{SHNC}})|/|k_{\text{eff}}^{\text{Ref}}| \times 10^5$, which is used in most criticality calculations.

From Table 8 we observe that there is a good agreement between the P_7 SHNC k_{eff} solutions and the k_{eff} computed with the reference methods (MCNP4C, S_8 and P_n). We find differences in pcm ranging from 10.2 pcm (P_n) to 95.1 pcm (MCNP4C) for Case 1, and the differences for Case 2 ranging from 30.1 pcm (S_8) to 102.8 (P_n).

The P_7 k_{eff} solutions are within 1σ uncertainty (Monte Carlo statistics) of MCNP4C results. For this problem, P_7 angular approximations are sufficient to obtain accurate transport solutions and also the spatial mesh of 5 cm intervals used provides satisfactory results.

Another advantage of the nodal collocation method is that we can also obtain the subcritical modes, as shown in Table 9 for the P_7 approximation ($M = 5$) for this particular problem.

4.3.2 Benchmark problem 2

The second benchmark problem considered is a small core model of a Fast Breeder Reactor (FBR). The model is calculated in 4 energy groups, and the cross-sections are given in Takeda and Ikeda (1991). The overall dimensions of the system are $140 \times 140 \times 150$ cm. As it is shown in Fig. 8, the model is comprised of a fuel region, radial and axial blankets and a control rod region.

Table 8
Fine mesh SHNC k_{eff} predictions for different angular P_L approximations and $M = 5$, compared with various reference methods for the benchmark problem 1

Method	Case 1	Case 2
MCNP4C	0.97763(±0.0013)	0.96221(±0.0013)
S_8	0.9772 (±0.0001)	0.9623 (±0.0001)
P_n	0.9766 (±0.0006)	0.9630 (±0.0008)
SHNC P_1	0.92878	0.93242
P_3	0.97312	0.96118
P_5	0.97586	0.96192
P_7	0.97670	0.96201

Table 9
Four dominant eigenvalues for the P_7 approximation for the benchmark problem 1 (cases 1 and 2)

Eigenvalues	P_7 (Case 1)	P_7 (Case 2)
k_{eff}	0.97670	0.96201
2nd	0.69911	0.70010
3rd	0.69239	0.68843
4th	0.68040	0.65124

Vacuum boundary conditions are applied. For this model, we have considered

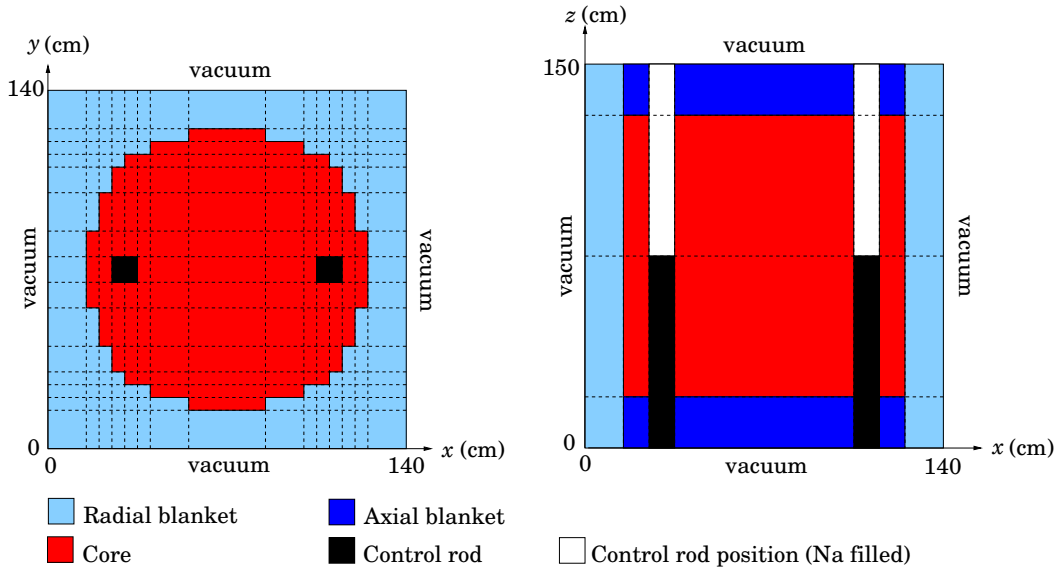

Fig. 8. Configuration of 3D benchmark problem 2. Dashed lines correspond to the spatial discretization according with the material zones.

two cases: Case 1), the control rods are withdrawn (the control rod position

is filled with Na) and Case 2), the control rods are half-inserted.

Table 10 presents the nodal collocation method (SHNC) solutions for k_{eff} eigenvalue for $P_1 - P_7$ approximations, using the coarse mesh computation (spatial discretization according with material zones, see dashed lines in Fig. 8). The number of meshes are 15, 15 and 4 in X, Y and Z directions, respectively, resulting in a total number of 900 3D nodes. In previous calculations (Takeda and Ikeda, 1991) one quarter of the reactor was taken and the reference mesh size adopted was 5 cm, resulting in 5880 3D nodes. We observe that for this problem, the SHNC gives satisfactory results in comparison with the EVENT solutions, and it does not require a smaller mesh size. This is because the thermal neutron flux is small compared to that in problem 1 and the angular flux distribution is nearly isotropic.

Table 10
Coarse mesh solutions for k_{eff} eigenvalue for different P_L approximations, for the benchmark problem 2, Case 1

Method	SHNC			EVENT
M	3	4	5	
P_1	0.96820	0.96819	0.96819	0.96875
P_3	0.97102	0.97240	0.97280	0.97335
P_5	0.97108	0.97247	0.97293	0.97345
P_7	0.97111	0.97249	0.97298	0.97348

Table 11 presents the SHNC solutions for k_{eff} eigenvalue using the same P_L approximations, for the benchmark problem 2, Case 2. We have also considered the coarse mesh discretization and different orders M of the expansion of the fields.

Table 11
Coarse mesh solutions for k_{eff} eigenvalue for different P_L approximations, for the benchmark problem 2, Case 2

Method	SHNC			EVENT
M	3	4	5	
P_1	0.95369	0.95351	0.95344	0.95380
P_3	0.95692	0.95831	0.95872	0.95908
P_5	0.95700	0.95843	0.95889	0.95924
P_7	0.95702	0.95846	0.95893	0.95928

In Figs. 9 and 10 we compare the four-group scalar fluxes along the x-axis from core centre for sucessive SHNC P_L approximations, for Cases 1 and 2,

with polynomial order $M = 5$.

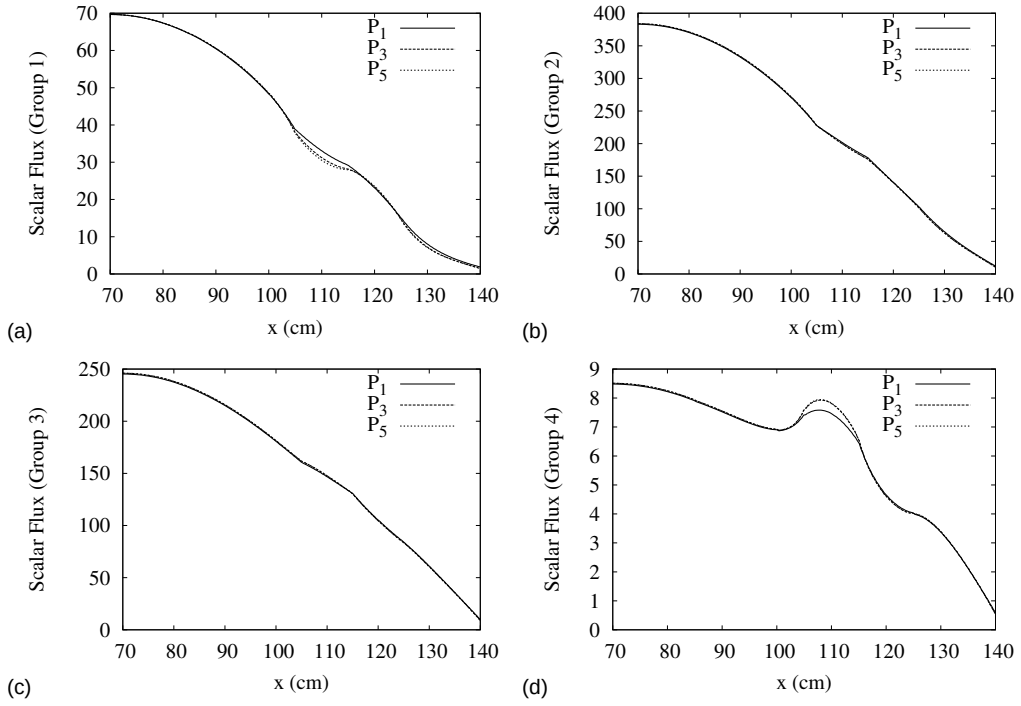

Fig. 9. Comparison of scalar flux of SHNC P_1-P_5 approximations for control rod-out (Case 1) of benchmark problem 2, from core centre of coordinates (70,70,74.5) to (140,70,74.5). (a) Energy group 1. (b) Energy group 2. (c) Energy group 3. (d) Energy group 4.

Table 12 shows a comparison between the SHNC P_L results for k_{eff} and the k_{eff} reference solutions obtained with the MCNP4C code (Ziver et al., 2005) and the mean values of k_{eff} calculated by various 3D transport code methods as reported in Takeda and Ikeda (1991), for the benchmark problem 2, Case 1 and Case 2.

The SHNC k_{eff} eigenvalues from P_7 approximation show differences against S_8 reference solutions of 43.1 pcm for Case 1, and 38.5 pcm for Case 2. Also we find differences against S_4 of 53.4 pcm for Case 1 and 49 pcm for Case 2, and the differences against MCNP4C are 65.7 pcm and 95.8 pcm for Case 1 and Case 2, respectively. In all cases, the differences are within 100 pcm. We observe that P_5 and P_7 k_{eff} eigenvalues from SHNC are within 2σ uncertainty of MCNP4C results.

Finally, we have obtained the subcritical modes for this problem 2, as it is shown in Table 13, for the P_7 approximation ($M = 5$).

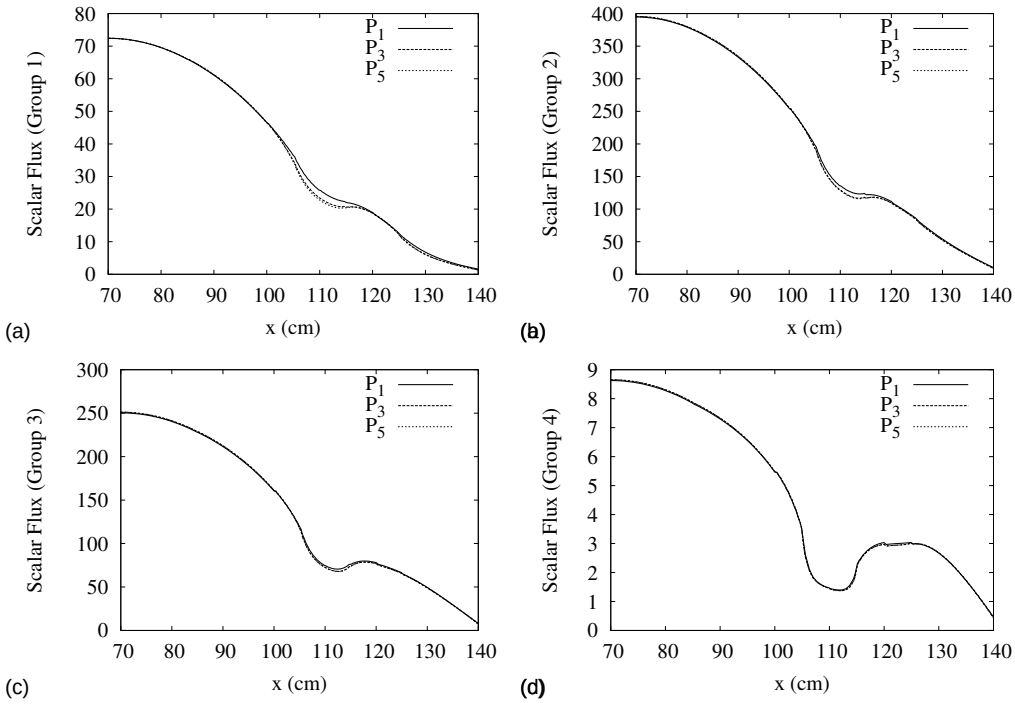

Fig. 10. Comparison of scalar flux of SHNC P_1-P_5 approximations for control rod-in (Case 2) of benchmark problem 2, from core centre of coordinates (70,70,74.5) to (140,70,74.5). (a) Energy group 1. (b) Energy group 2. (c) Energy group 3. (d) Energy group 4.

Table 12
Coarse mesh SHNC k_{eff} predictions for different angular P_L approximations, compared with various reference methods, for the benchmark problem 2

Method	Case 1	Case 2
MCNP4C	0.97362($\pm$0.0008)	0.95985($\pm$0.0008)
S_4	0.9735 ($\pm$0.0001)	0.9594 ($\pm$0.0001)
S_8	0.9734 ($\pm$0.0002)	0.9593 ($\pm$0.0002)
SHNC P_1	0.96819	0.95344
P_3	0.97280	0.95872
P_5	0.97293	0.95889
P_7	0.97298	0.95893

5 Conclusions

We have reviewed the multi-dimensional spherical harmonics equations (P_L) and applied a nodal collocation method for the spatial discretization of these equations based on the expansion of the angular neutronic moments in terms of orthonormal Legendre polynomials. The main advantage of the method

Table 13
Four dominant eigenvalues for the P_7 approximation for the benchmark problem 2 (Cases 1 and 2)

Eigenvalues	P_7 (Case 1)	P_7 (Case 2)
k_{eff}	0.97298	0.95893
2nd	0.77109	0.76390
3rd	0.74930	0.75053
4th	0.73244	0.71007

is the lower dimension and good characteristics of the matrix associated to the algebraic problem. The method is able to work with nodes of big size using high-order Legendre polynomials giving satisfactory results. The coarse mesh computation and the serendipity approximation drastically reduce the dimension of the algebraic problem in comparison to other methods like finite elements or finite differences.

The nodal collocation method has been implemented in a FORTRAN 90 code called SHNC, and applied to two one-group homogeneous 2D and 3D cases and to two multi-group 3D benchmark problems. The results of the homogeneous cases are compared with the ones obtained with the DANTSYS code, observing a convergence of the P_L k_{eff} eigenvalue to the reference solution practically with order $L = 5$. For the 3D benchmark problems studied, coarse mesh angular approximations greater than P_5 give accurate transport solutions quite similar to the ones obtained with other codes like EVENT and MCNP4C. Also the results obtained with SHNC reproduce the reference solution of the benchmark cases presented by Takeda and Ikeda.

Acknowledgements

This work has been partially supported by the Spanish Ministerio de Educación y Ciencia under projects ENE2008-02669, the Generalitat Valenciana under project ACOMP/2009/058, and the Universidad Politécnica de Valencia under project PAID-05-09-4285.

References

Alcouffe, R. E., Baker, R. S., Brinkley, F. W., Marr, D. R., O'Dell, R. D., Walters, W. F, 1995. DANTSYS: A diffusion accelerated neutral particle transport code system. Los Alamos National Laboratory, LA-12969-M.

Brantley, P. S., Larsen, E. W., 2000. The simplified P_3 approximation. Nucl. Sci. Eng., 134:1–21.

Briesmeister, J. F., 2000. MCNP–A general Monte Carlo N-particle transport code, version 4C. Technical Report LA-13709-M, Los Alamos National Laboratory.

Capilla, M., Talavera, C. F., Ginestar, D., Verdú, G., 2005. A nodal collocation method for the calculation of the lambda modes of the P_L equations. Ann. Nucl. Energ., 32:1825–1853.

Capilla, M., Talavera, C. F., Ginestar, D., Verdú, G., 2008. A nodal collocation approximation for the multidimensional P_L equations - 2D applications. Ann. Nucl. Energ., 35:1820–1830.

Clark, M. Jr., Hansen, K. F., 1964. Numerical Methods of Reactor Analysis. New York Academic, New York.

Davison, B., 1957. Neutron Transport Theory. Oxford University Press, London.

de Oliveira, C. R. E., Eaton, M. D., Umpleby, A. P., Pain, C. C., 2001. Finite element spherical harmonics solutions of the 3D Kobayashi benchmarks with ray-tracing void treatment. Prog. Nucl. Energy, 261 (39):243–261.

Fletcher, J. K., 1983. A solution of the neutron transport equation using spherical harmonics. J. Phys. A: Math. Gen., 16:2827–2835.

Gelbard, E. M., 1968. Spherical harmonics methods: P_L and double P_L approximations. Computing Methods in Reactor Physics. Kelberg, D., Okrent, C. N. (eds.). Gordon and Breach, New York.

Hébert, A., 1987. Development of the nodal collocation method for solving the neutron diffusion equation. Ann. Nucl. Energ., 14(10):527–541.

Rhoades, W.A., Childs, R.L., 1993. DORT/TORT two- and three-dimensional discrete ordinates transport, Version 2.7.3. ORNL, Oak Ridge, RSIC-CCC-543.

DeHart, M.D., 2009. NEWT: A new transport algorithm for two-dimensional discrete ordinates analysis in non-orthogonal geometries. ORNL/TM-2005/39.

Sjoden, G. E., Haghighat, A., 1996. PENTRAN, A 3-D scalable transport code with complete phase space decomposition. Trans. Am. Nucl. Soc., p. 74.

Stacey, W. M., 2001. Nuclear Reactor Physics. Wiley, New York.

Takeda, T., Tamitani, M., Unesaki, H., 1988. Proposal of 3-D neutron transport benchmark problems. Technical Report A-953, Rev. 1.

Takeda, T., Ikeda, H., 1991. 3-D neutron transport benchmarks. Technical Report OECD/NEA. Committee on Reactor Physics (NEACRP).

Tomasević, D. I., Larsen, E. W., 1996. The simplified P_2 approximation. Nucl. Sci. Eng., 122:309–325.

Verdú, G., Ginestar, D., Vidal, V., Muñoz-Cobo, J. L., 1994. λ modes of the neutron diffusion equation. Ann. Nucl. Energ., 21(7):405–421.

Weinberg, A. M., Wigner, E. P., 1958. The Physical Theory of Neutron Chain Reactors. Chicago University Press, Chicago.

Ziver, A. K., Shahdatullah, M. S., Eaton, M. D., Oliveira, C. R. E., Umpleby, C. C., Goddard, A. J. H., 2005. Finite element spherical harmonics (P_N) solutions of the three-dimensional Takeda benchmark problems. Ann. Nucl. En. 32:925-948.